NACA

RESEARCH MEMORANDUM

PRESSURE MEASUREMENTS AT SUPERSONIC SPEEDS ON A

SECTION OF A RECTANGULAR WING HAVING AN
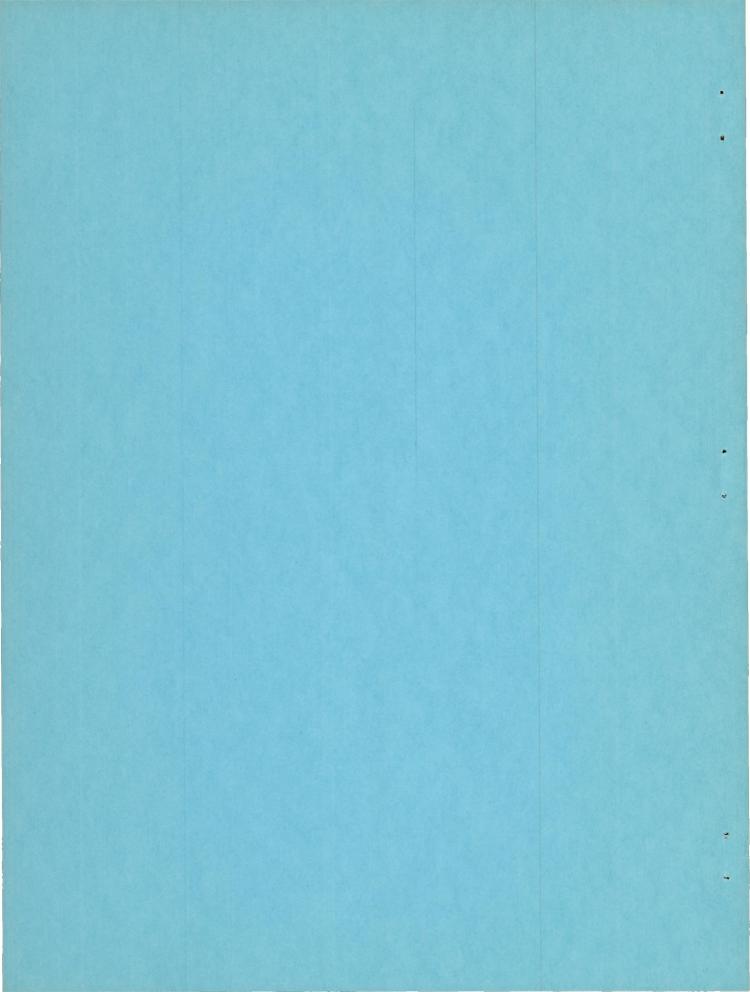
NACA 65-009 PROFILE

By Robert W. Rainey

Langley Aeronautical Laboratory
Langley Air Force Base, Va.

NATIONAL ADVISORY COMMITTEE
FOR AERONAUTICS
WASHINGTON
March 10, 1950

NATIONAL ADVISORY COMMITTEE FOR AERONAUTICS

RESEARCH MEMORANDUM

PRESSURE MEASUREMENTS AT SUPERSONIC SPEEDS ON A

SECTION OF A RECTANGULAR WING HAVING AN

NACA 65-009 PROFILE

By Robert W. Rainey

SUMMARY

An investigation of a rectangular wing with a subsonic-type round-leading-edge airfoil section (NACA 65-009) was made at Mach numbers of 1.62, 1.93, and 2.40 and at a Reynolds number of about 1.00×10^6. The results obtained indicated good agreement, except within the laminar-separated region on the low-pressure surface of the model, between the experimental pressure distributions and those calculated by an approximate method.

The experimental normal-force and pitching-moment coefficients varied almost linearly with angle of attack up to the limit of the tests, but the corresponding slopes were less than those for a symmetrical circular-arc airfoil of the same thickness ratio. The pressure drag of the NACA 65-009 airfoil was considerably greater than that of the symmetrical circular-arc airfoil throughout the range of test Mach numbers and varied from 1.4 times greater at a Mach number of 1.62 to 2.1 times greater at a Mach number of 2.40.

INTRODUCTION

Rocket flight tests at transonic and moderate supersonic speeds have indicated the zero-lift drag of a wing having NACA 65-009 airfoil sections to be lower than that of a wing having circular-arc sections and the same thickness ratio (reference 1). This result was obtained for Mach numbers from just below one to about $M = 1.3$ and the maximum difference in drag occurred at $M = 1$, this difference decreasing to about zero at $M = 1.3$. It was thus indicated that airfoil sections having round leading edges might be desirable for flight near $M = 1$. At higher supersonic speeds, it is fairly obvious that the drag of the round-leading-edge section would be greater; however, little data are

available to assess the magnitude of the increase, and only semiempirical means exist for estimating the pressures over the round-leading-edge section. The present investigation was therefore made to provide data on the pressures about a round-leading-edge section at higher supersonic speeds so that quantitative drag values could be obtained, and experimental data would be available as an aid in the development of suitable methods for predicting pressures over airfoils with detached shocks.

In the tests, pressure measurements were made on a model wing having an NACA 65-009 airfoil section and were made at a station on the wing where the flow was believed to be essentially two dimensional. The tests were made in the Langley 9-inch supersonic tunnel at Mach numbers of 1.62, 1.93, and 2.40 and Reynolds numbers of 1.07×10^6, 0.97×10^6, and 0.81×10^6, respectively. The results of the tests are compared with similar results from another investigation of a symmetrical circular-arc airfoil section also of 9-percent-thickness ratio. (See reference 2.) The measured pressures and integrated characteristics of the NACA 65-009 airfoil section are also compared with those predicted by an approximate method.

SYMBOLS

b' spanwise location of orifices

c chord of wing

c_c section chord-force coefficient $\left(\dfrac{\text{Chord force}}{q_1 c}\right)$

c_{d_p} section pressure-drag coefficient

c_m section pitching-moment coefficient about the half-chord $\left(\dfrac{\text{Moment about half-chord}}{q_1 c^2}\right)$

c_{m_α} variation of section pitching-moment coefficient with angle of attack $\left(\dfrac{dc_m}{d\alpha}\right)$

c_n section normal-force coefficient $\left(\dfrac{\text{Normal force}}{q_1 c}\right)$

c_{n_α} variation of section normal-force coefficient with angle of attack $\left(\dfrac{dc_n}{d\alpha}\right)$

M_1 free-stream Mach number

p local static pressure on surface of airfoil

p_1 free-stream static pressure

p_s total-head pressure behind normal shock wave

P pressure coefficient $\left(\dfrac{p - p_1}{q_1}\right)$

P_{sonic} pressure coefficient for sonic speed

P_{max} pressure coefficient behind normal shock wave $\left(\dfrac{p_s - p_1}{q_1}\right)$

q_1 free-stream dynamic pressure $\left(\dfrac{\gamma}{2} p_1 M_1{}^2\right)$

R Reynolds number $\left(\dfrac{\rho V c}{\mu}\right)$

V free-stream velocity

α angle of attack with respect to stream

μ coefficient of viscosity

ρ mass density of the free stream

APPARATUS AND TEST METHODS

Wind Tunnel

All tests were conducted in the Langley 9-inch supersonic tunnel, which is of the continuous-operating, closed-return type in which the pressure and humidity can be controlled. During these tests the amount of water vapor in the tunnel air was kept sufficiently low so that the effects of condensation in the supersonic nozzle were negligible. The Mach number was varied by interchanging nozzle blocks which form test sections approximately 9 inches square. Eleven fine-mesh screens are installed in the settling chamber ahead of the nozzle to aid in damping out turbulence.

Model

The model had a rectangular plan form with a square tip and was of all-steel construction with 14 static-pressure orifices in each surface and one orifice located at zero percent chord. Within the first 7.2 percent chord of the airfoil were located nine orifices, which made it possible to determine accurately the experimental pressure distribution within the nose region. (See fig. 1.) The model was mounted from a plate which could be rotated to change the wing angle of attack. The stream surface of this plate was flush with the side wall of the tunnel as shown in figure 2.

It is believed that the model was constructed to within ±0.004 inch of the specifications with the exception of the nose section, which was at a slight positive angle of attack with respect to the remainder of the airfoil section. It was determined from the tests that the amount of camber was so slight that its effect on the pressures about the remainder of the airfoil was negligible.

Since a boundary-layer plate was not utilized to bypass the boundary layer, it was reasonable to expect that a root interference would occur at the junction of the leading edge of the model and the tunnel-wall boundary layer. The model was designed so that the orifice station could be located free of the root interference, as indicated in figure 2. The spanwise location of the orifice station with respect to the root interference was determined experimentally before taking any pressure-distribution measurements, as explained subsequently. By estimating the extent to which the influence due to the tip would be felt in supersonic flow and by locating the orifice station a reasonable spanwise distance inboard of the point at which the region of influence crossed the trailing edge, it is believed that the orifice station was relatively free of tip effects.

Test Methods

Pressure-distribution measurements.- In order that the orifice station might be placed within the region of flow free of the root interference, the first test at each Mach number consisted of finding this location experimentally. This was accomplished by setting the model at the design maximum angle of attack and displacing the model laterally in both directions; thereby, the spanwise location of the orifice station was varied with respect to the tunnel wall. After noting the position at which the last chordwise orifice intersected the region of the root interference, the model was again displaced laterally; this displacement resulted in the movement of the orifice station to a test location that was a reasonable distance away from the region of root interference.

Systematic pressure-distribution measurements were made by varying
the angle of attack positively and negatively from zero angle of attack.
The maximum angles of attack for the tests were limited by a combination
of structural and aerodynamical considerations and at Mach numbers of 1.62,
1.93, and 2.40 were 10°, 12°, and 15°, respectively. At each angle of
attack the static pressures on the wing and the total pressure in the
tunnel settling chamber were indicated on a multitude mercury manometer
and recorded simultaneously by photographing the manometer.

Through the use of a film reader, the pressures on the airfoil were
read directly from the film record as pressure coefficients. The normal-
force, pitching-moment, and pressure-drag values were obtained by
mechanically integrating the faired pressure-distribution curves.

Shadowgraphs.- By reflecting parallel light into the plane of the
wing, it was possible to observe on the tunnel wall a shadowgraph of the
flow about the model. With the optical setup used, it was not possible
to photograph the shock and expansion phenomena about the front and rear
of the model simultaneously. The photographs taken through the observa-
tion window opposite the model were oblique with respect to the parallel
light, as was obviously necessary to avoid blocking the light; conse-
quently, the flow about the nose is not seen. In order to show the
shadow images in the region of the nose, other photographs, still more
oblique with respect to the model axis and parallel light, were taken
through an upstream observation window. Since the camera could not be
located along the axis of the model, the true angles of the shocks and
expansions cannot be obtained from the photographs.

It was expected that the shadowgraphs obtained by this technique
were not a true indication of the approximate two-dimensional flow,
since the light also traversed the regions of density changes in the
root interference and tip regions. In order to qualitatively judge the
extent to which the image indicates the two-dimensional flow, observa-
tions of the image were made for various wing spans. Because the root-
interference region is adjacent to the tunnel wall, it was expected to
be relatively ineffective in producing sharp shadow images of
sufficient density to be photographed. Variation of the wing span
changed the relative portion of the approximate two-dimensional flow
over the wing, as well as changing the distance of the tip region from
the tunnel wall. Had there been a noticeable deviation of the light
rays as they passed through the tip region, there would have been a
change in the intensity and location of the shadow images on the tunnel
wall as the span was varied. No such changes were evident by varying
the span from a projection from the wall of 2.5 chords to a projection
of 1.5 chords; therefore, it was indicated that the effects upon the
shadowgraphs of the tip regions were negligible.

PRECISION OF DATA

The individual pressure coefficients are believed to be accurate
within ±0.01 at all Mach numbers. The pressures at any orifice that
seemed to be consistently erroneous were discarded. A summary of the
maximum probable error in each of the quantities involved in the data
is given in the following table:

M_1	Angle of attack (deg)	c_n	c_m	c_{d_p}
1.62 1.93 2.40	±0.05	±0.007	±0.001	±0.0008

For the region of the test section that would influence the flow
over the model, the maximum stream static variation was ±1 percent and
the maximum Mach number variation was ±0.01; these are the results of
empty-test-section surveys. From tests of the model at angles of attack
of 0°, 1°, and 2°, laminar separation was observed to occur behind the
last orifice. For these cases the points of separation for use in
fairing the pressure-distribution curves to the trailing edge were taken
from the shadowgraphs; this minimized the errors in the integrated c_n
and c_m values at these low angles of attack.

RESULTS AND DISCUSSION

Calculation of the Pressure Distributions

The calculated pressure-distribution curves presented in figures 3
to 5 were based upon the assumption, as in the linear theory, that the
pressure coefficient is zero ($p = p_1$) on the airfoil surface where the
tangent to the surface is parallel to the free-stream direction. The
Prandtl-Meyer expansion theory was then applied forward until sonic
velocity was reached and rearward to the trailing edge. It was also
assumed that the stagnation point was located at the leading edge and
that the pressure coefficient at the leading edge was equal to the
pressure coefficient at stagnation behind a normal shock P_{max}. The
pressure-coefficient curves were faired from P_{max} to the coefficient at
the sonic line P_{sonic} a chordwise distance of less than 6 percent chord
at all angles of attack for which the curves were calculated. This method

of approximation differs from that used in reference 3 within the region between the leading edge and where the tangent to the airfoil surface is parallel to the free stream.

Experimental Pressure Distributions

In figures 3 to 5 are presented the experimental pressure-distribution curves. It is apparent that the nose section of the airfoil had a slight positive angle, as indicated by comparing the upper- and lower-surface pressures of the $\alpha = 0^\circ$ curves. This differential in surface pressures resulted in an integrated normal-force coefficient at $\alpha = 0^\circ$ and was found to be 0.007 or less. As the pressures aft of the nose section on the upper and lower surfaces were equal within experimental accuracy, the effects of the nose section upon the remainder of the airfoil appeared negligible. The pressure coefficient at the leading edge was in good agreement with the calculated value P_{max} even at the higher angles of attack; this indicated little movement in the stagnation point at the Mach numbers and angles of attack tested.

The laminar-separated regions are indicated in figures 3 to 5 by the portion of the curves the pressure gradient of which is very nearly zero. Throughout the range of angles of attack the point of separation on the low-pressure surface moved forward as the angle of attack increased. A closer analysis of the pressure-distribution curves revealed that the laminar separation occurred farther forward on the airfoil at the higher Mach numbers, this fact appearing at first to be in contradiction to the results presented in reference 4, which showed a rearward movement of the separation point with increase in Mach number, Reynolds number remaining constant. In the present paper the laminar boundary layer and point of separation can be affected not only by change in Mach number but also in Reynolds number, the pressure ratio across the shock originating just behind the trailing edge, and the pressures on the high-pressure surface of the model.

It was noted that the pressures just upstream and downstream of the point of separation vary but slightly despite the first leg of the λ-shock that is prevalent with laminar separation intersecting the boundary layer in that region (see reference 5). There was no evidence of any turbulent boundary layer which is characterized by an abrupt increase in pressure where the one strong shock wave intersects the boundary layer, as shown in reference 6.

The shape of the experimental curves agrees well with the calculated curves except throughout the laminar-separated regions. At low α's at every Mach number tested, the pressure coefficient at the leading edge was within ±0.02 of the calculated value. The experimental pressure coeffi-cients were consistently more positive than the calculated values at the

point where the airfoil surface was tangent to the free stream by an
amount never greater than 0.03, as shown in figures 3 to 5 for the
range of $\alpha = 0^\circ$ to $\alpha = 4^\circ$. This was expected, in that the effects
upon the pressure distribution of the changes in entropy through
the bow wave were neglected. Since good agreement between the calculated
and experimental pressure coefficients was indicated, good agreement
between the aerodynamic characteristics could be expected.

Aerodynamic Characteristics

In figures 6 to 14 are presented the integrated aerodynamic
characteristics. Due to the slight cambered effect of the model, the
curves are displaced slightly, for which no correction has been applied.
The slopes of all the normal-force and pitching-moment curves along with
the center-of-pressure locations are given in table I for the NACA 65-009
and the symmetrical circular-arc airfoils.

Section normal-force coefficients.- The experimental normal-force
coefficients of the NACA 65-009 airfoil varied linearly with α up to
an angle of attack of approximately 10°, the maximum angle of attack
tested at $M = 1.62$ (see figs. 6 to 8). At $M = 1.93$ and 2.40 c_{n_α}
increased slightly above an α of about 11°. Plots of c_n at
negative and positive angles of attack revealed that the c_n curves were
symmetrical about the angle of zero normal force. The experimental c_{n_α}
of the symmetrical circular-arc airfoil was about 10 percent greater
than c_{n_α} for the NACA 65-009 airfoil at $M = 1.62$ (see reference 2).

The calculated values of c_n varied linearly with α, and the
calculated values of c_{n_α} were greater than the experimental values at
every Mach number tested; however, they agreed within about 3 percent.
The linear flat-plate values of c_{n_α} were also within 3 percent of the
experimental results (see table I).

Section pitching-moment coefficients.- The experimental c_m curves
presented in figures 6 to 8 revealed that the section pitching-moment
coefficients varied linearly with α except for $M = 2.40$ where c_{m_α}
increased slightly above an α of 12°. The experimental c_{m_α} for
the symmetrical circular-arc airfoil was about 29 percent greater than
that for the NACA 65-009 airfoil at $M = 1.62$.

The calculated moment curves varied linearly with α and were in good
agreement with the experimental values except at $M = 1.62$, where the
agreement was fair.

Variation of c_m with c_n.- Plots of c_m as a function of c_n
in figures 9 to 11 indicated that there existed a linear variation

throughout the range of angles of attack and Mach numbers tested. The

values of $\dfrac{dc_m}{dc_n}$ were found to be approximately 0.078, 0.078, and 0.091

for M = 1.62, 1.93, and 2.40, respectively, which indicated that as the
stream Mach number increased, the center of pressure moved forward from
the 42.2 percent to the 40.9 percent chord. At M = 1.62, the center-of-
pressure location for the symmetrical circular-arc airfoil was at the
41.0 percent chord.

   Section pressure-drag coefficients.- The experimental c_{d_p} values
have been calculated from the experimental c_n and c_c values for the
NACA 65-009 airfoil, and a comparison is made in figures 12 and 13 with
the theoretical pressure-drag coefficients of a symmetrical circular-
arc airfoil section of the same thickness ratio. In order to show the
departure from the theoretical values to be expected for the circular-
arc airfoil section, experimental data were taken from reference 2 and
compared with the theoretical chordwise pressure distribution at $\alpha = 0^{\circ}$
and M = 1.62. This comparison is shown in figure 14. The theoretical
and experimental chordwise pressure distributions are in excellent
agreement except within the laminar-separated region near the trailing
edge. The separation decreases the expansion in that region; consequently,
the experimental pressure drag is less than the theoretical values, as
indicated in figure 12. However, the experimental pressure drag is of
the same order as the theoretical pressure drag - the difference due to
laminar separation being about 5 percent; thus, the theoretical
pressure drags are used as a basis of comparison in the present paper.

   A comparison of the pressure drags of the two airfoils at M = 1.62
(see fig. 13) indicates that the pressure drag of the NACA 65-009 airfoil
is much greater than that of the symmetrical circular-arc airfoil. This
difference in pressure drag was found to decrease as α increased. At
$\alpha = 0^{\circ}$ (see fig. 12) the pressure drag of the NACA 65-009 section was 1.4,
1.6, and 2.1 times greater than the drag of the symmetrical circular-arc
section at Mach numbers of 1.62, 1.93, and 2.40, respectively. Since the
chordwise pressure distributions of the two airfoils were relatively
similar with the exception of the nose region (see fig. 14), the difference
in pressure drags is attributed primarily to the high pressures experienced
by the subsonic-type round leading edge of the NACA 65-009 airfoil.

                               Shadowgraph Studies

   The shadowgraphs of the NACA 65-009 airfoil at $\alpha = 10^{\circ}$, M = 2.40,
are presented in figure 15. With the optical setup used, it was
impossible to photograph both front and rear portions simultaneously. In
figures 15(a) and 15(b) the detached bow wave is apparent and is composed
of a normal shock wave just ahead of the leading edge of the model, with

the shock wave sloping rearward as the expansions emitted from both surfaces decrease the angle of the bow wave. The shock appearing just behind the upper portion of the bow wave originated at the leading edge of the tip and reflected off the window opposite the model, the image being caused by the intensified gradient at the point of reflection.

A schematic drawing of the shadowgraphs of the flow past the model is presented in figure 16. At approximately the 55 percent chord of the low-pressure surface the flow separated, deflecting away from the model. A weak oblique shock, characteristic of laminar separation, originated at the point of separation and is visible in the shadowgraph. A comparison with the pressure-distribution curve at $\alpha = 10^\circ$, M = 2.40, indicated that the region of laminar separation as indicated by shadowgraphs and pressure measurements is coincident.

On the lower surface there is no evidence of separation. As the flow passes beyond the trailing edge, it overexpanded beyond the stream direction to a velocity greater than that of free stream. The expansions are visible as rays originating at the trailing edge. A mixing line is visible between the laminar-separated region of the low-pressure surface and the overexpanded flow. Just downstream of the trailing edge the overexpanded flow turns streamwise, causing an oblique shock wave. Likewise, the flow adjacent to the laminar-separated region of the low-pressure surface turns streamwise, causing an oblique shock of the opposite family. Between these two shock waves the laminar-separated region has started mixing with the adjacent flow, becomes less distinct, and finally disappears entirely in the wake of the airfoil.

CONCLUDING REMARKS

An investigation of a rectangular wing with an airfoil section (NACA 65-009) with a subsonic-type round leading edge was made in the Langley 9-inch supersonic tunnel at Mach numbers of 1.62, 1.93, and 2.40 and at Reynolds numbers of about 1.00×10^6. The results obtained indicated good agreement, except within the laminar-separated regions, between the experimental pressure distributions and those calculated by an approximate method. Mechanical integration of the pressure distributions indicated that the experimental normal-force and pitching-moment coefficients for the test Mach numbers varied linearly with angle of attack up to $\alpha = 10^\circ$. The corresponding c_{n_α} and c_{m_α} were 10 percent

and 29 percent, respectively, less than those for a symmetrical circular-arc airfoil of the same thickness ratio. The experimental slopes for the NACA 65-009 were found to be in good agreement with the calculated values, with the exception of the slope of the pitching-moment-coefficient curve at M = 1.62. The pressure-drag coefficients were found to be about 41, 65, and 103 percent greater than the theoretical pressure-drag coefficients

of the symmetrical circular-arc airfoil at $\alpha = 0^{\circ}$ and at Mach numbers of 1.62, 1.93, and 2.40, respectively. The difference in pressure drags of the two airfoils was found to decrease as the angle of attack was increased. The center-of-pressure travel was small for all angles of attack and all Mach numbers tested. The boundary layer was basically laminar, and at a constant Mach number the point of separation moved forward as α increased. At constant α, the point of separation moved forward as M increased from 1.62 to 2.40.

Langley Aeronautical Laboratory
    National Advisory Committee for Aeronautics
        Langley Air Force Base, Va.

REFERENCES

1. Alexander, Sidney R.:   Drag Measurements of Symmetrical Circular-Arc
     and NACA 65-009 Rectangular Airfoils Having an Aspect Ratio of 2.7
     As Determined by Flight Tests at Supersonic Speeds.   NACA RM L6J14,
     1947.

2. Czarnecki, K. R., and Mueller, James N.:   Investigation at Mach
     Number 1.62 of the Pressure Distribution over a Rectangular Wing
     with Symmetrical Circular-Arc Section and 30-Percent-Chord Trailing-
     Edge Flap.   NACA RM L9J05, 1950.

3. Mayer, John P.:   Estimation of Lift and Drag of Airfoils at Near Sonic
     Speeds and in the Presence of Detached Shock Waves.   NACA RM L8L07,
     1949.

4. Ackeret, J., Feldmann, F., and Rott, N.:   Investigations of Compression
     Shocks and Boundary Layers in Gases Moving at High Speed.
     NACA TM 1113, 1947.

5. Liepmann, Hans Wolfgang: The Interaction between Boundary Layer and
     Shock Waves in Transonic Flow.   Jour. Aero. Sci., vol. 13, no. 12,
     Dec., 1946, pp. 623-638.

6. Liepmann, Hans Wolfgang, Askenas, Harry, and Cole, Julian D.:
     Experiments in Transonic Flow.   AF TR No. 5667, Air Materiel
     Command, Feb. 9, 1948.

TABLE I

TEST CONDITIONS, c_{n_α}, c_{m_α}, AND THE CENTER-OF-PRESSURE LOCATIONS

FOR THE NACA 65-009, THE SYMMETRICAL CIRCULAR-ARC,

AND INFINITE FLAT-PLATE AIRFOILS

M	R	b' (in.)	P_{max}	P_{sonic}
1.62	1.07×10^6	4.88	1.572	0.573
1.93	.97	4.38	1.644	.688
2.40	.81	4.38	1.711	.787

M	c_{n_α}	c_{m_α}	Center of pressure (percent chord)
NACA 65-009; Experimental			
1.62	0.0533	0.00414	42.2
1.93	.0419	.00328	42.2
2.40	.0320	.00291	40.9
NACA 65-009; Calculated			
1.62	0.0548	0.00474	41.4
1.93	.0428	.00330	42.3
2.40	.0310	.00298	40.4
Infinite flat-plate airfoil			
1.62	0.0548	-------	----
1.93	.0425	-------	----
2.40	.0320	-------	----
Symmetrical circular-arc airfoil (from reference 2)			
1.62	0.0587	0.0053	41.0
1.93	------	------	----
2.40	------	------	----

NACA
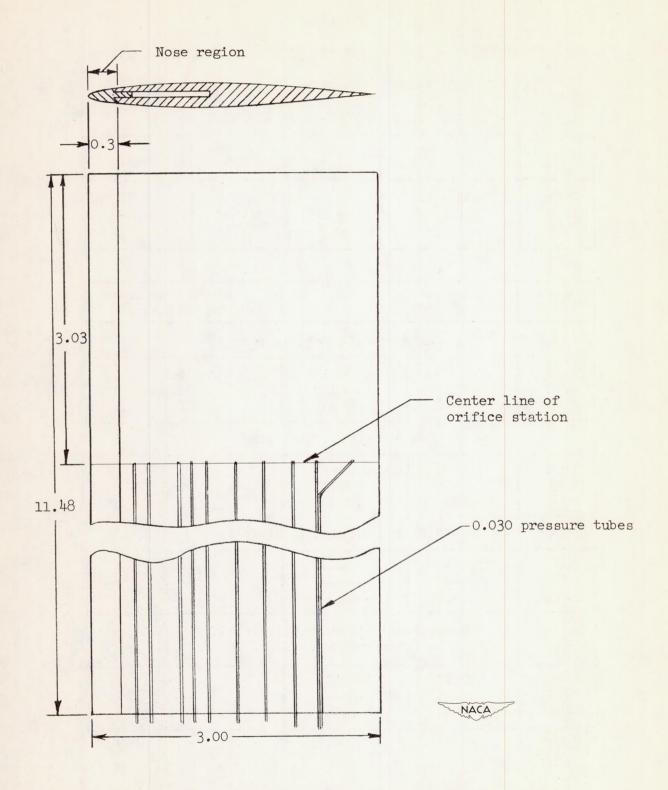
Figure 1.- Dimensional drawing of NACA 65-009 pressure-
distribution model.
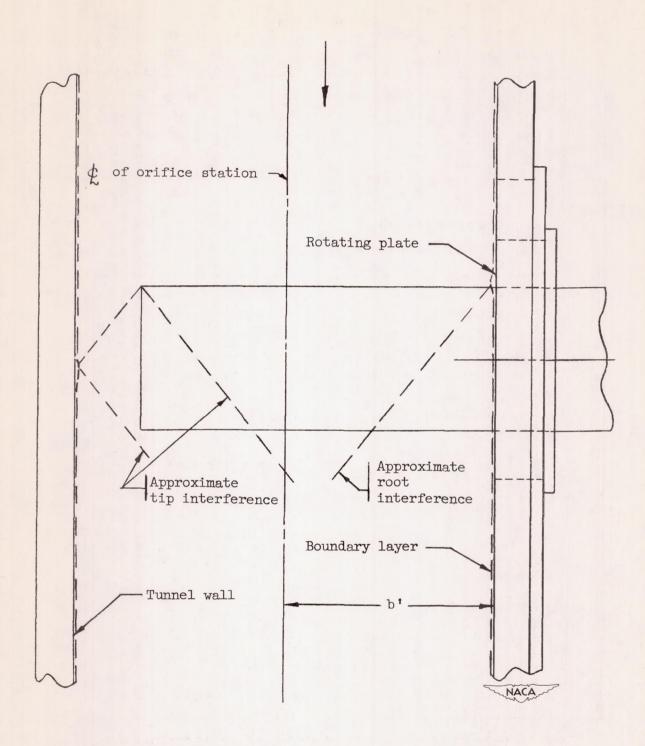
Figure 2.- NACA 65-009 pressure-distribution model mounted in the test section of the Langley 9-inch supersonic tunnel.
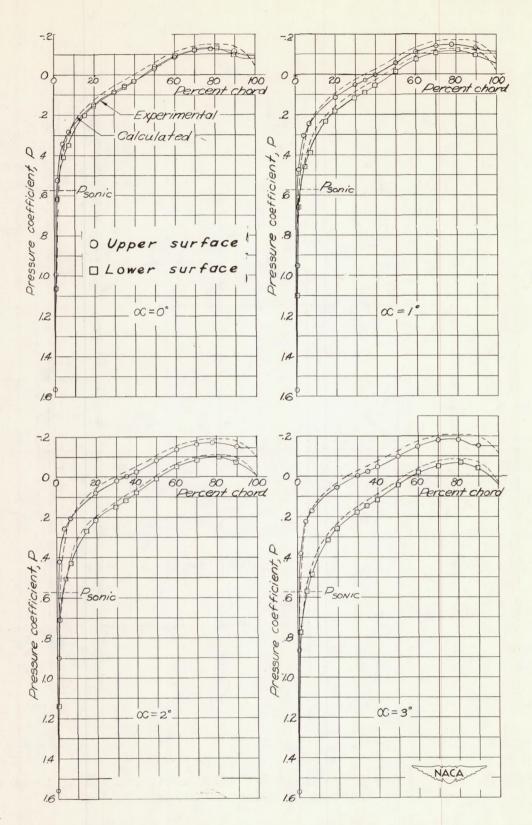
Figure 3.- Pressure distributions on NACA 65-009 airfoil at M = 1.62
and R = 1.07 × 10^6.
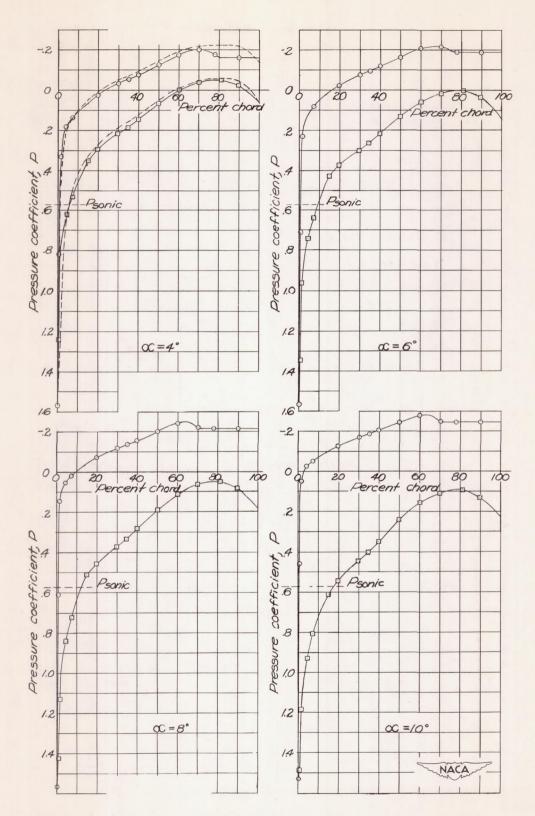
Figure 3.- Concluded.
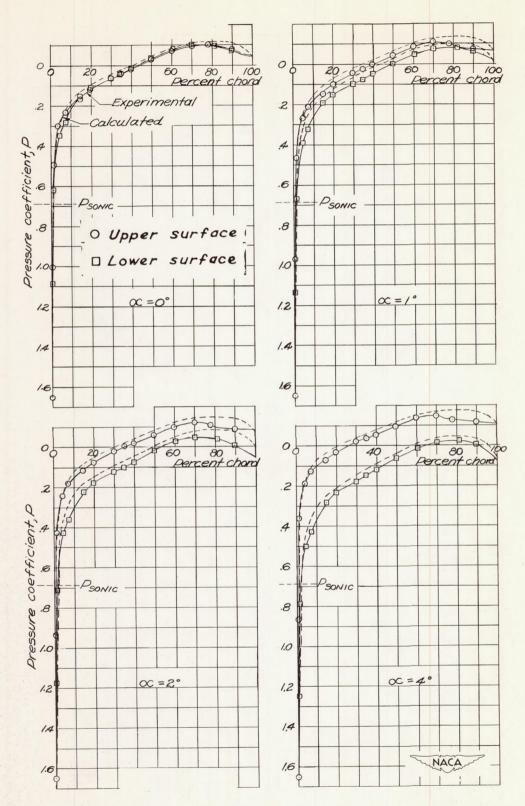
Figure 4.- Pressure distributions on NACA 65-009 airfoil at   M = 1.93
and   R = 0.97 × 10^6.
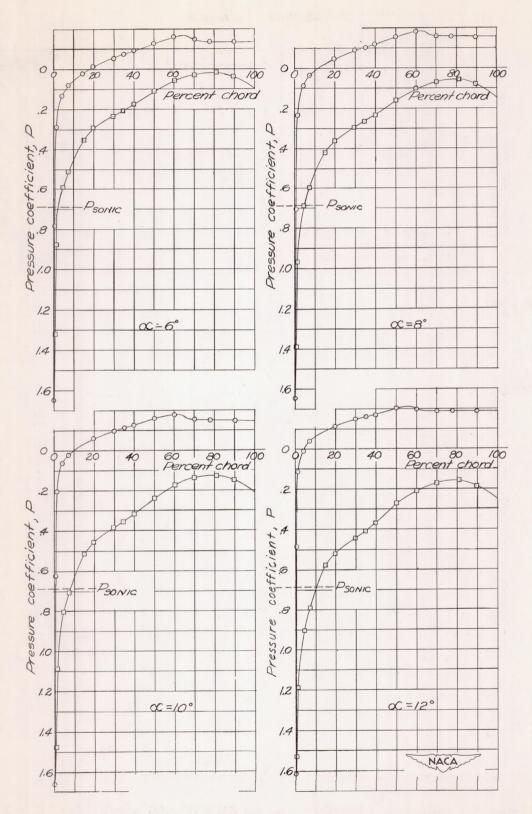
Figure 4.- Concluded.
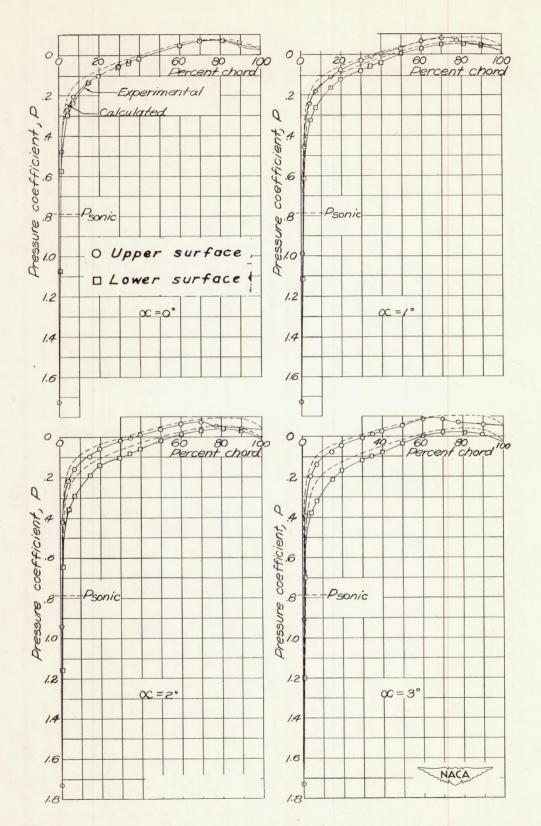
Figure 5.- Pressure distributions on NACA 65-009 airfoil at M = 2.40 and R = 0.81 × 10⁶.
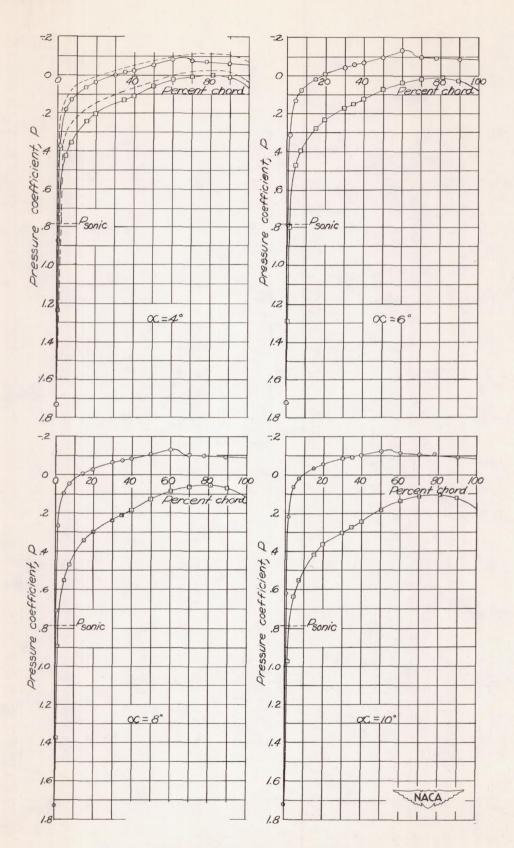
Figure 5.- Continued.
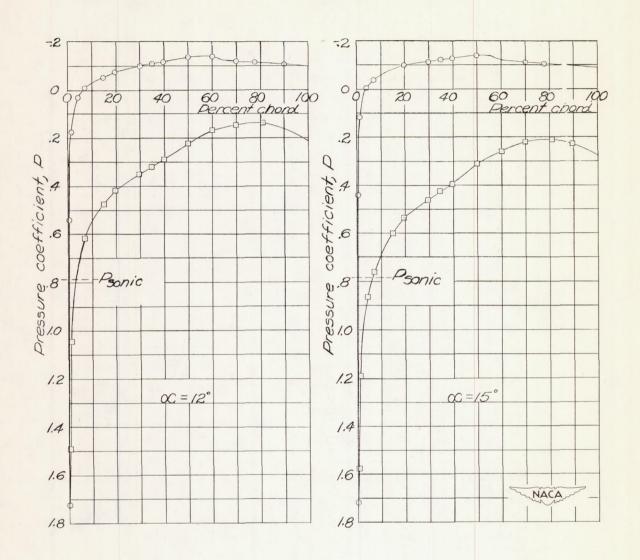
Figure 5.- Concluded.
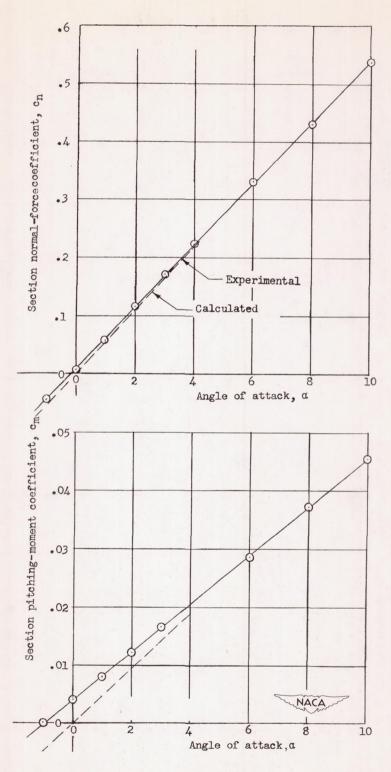
Figure 6.- Effect of angle of attack on section normal-force and
   pitching-moment coefficients for NACA 65-009. M = 1.62;
      R = 1.07 × 10^6.
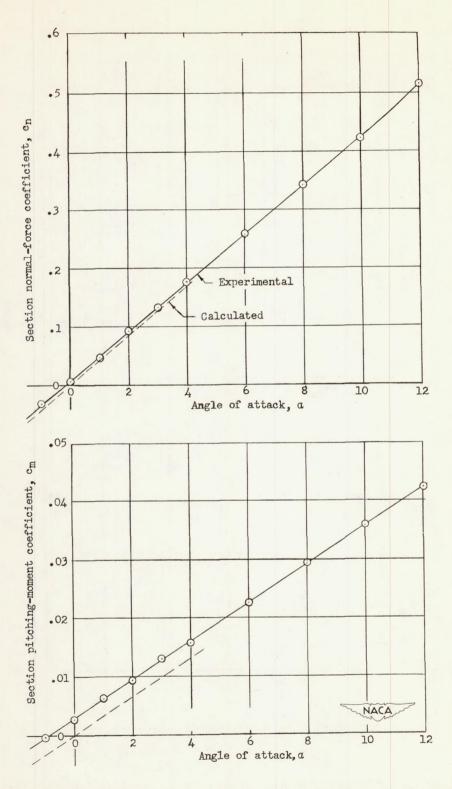
Figure 7.- Effect of angle of attack on section normal-force and pitching-moment coefficients for NACA 65-009. M = 1.93; R = 0.97 × 10^6.
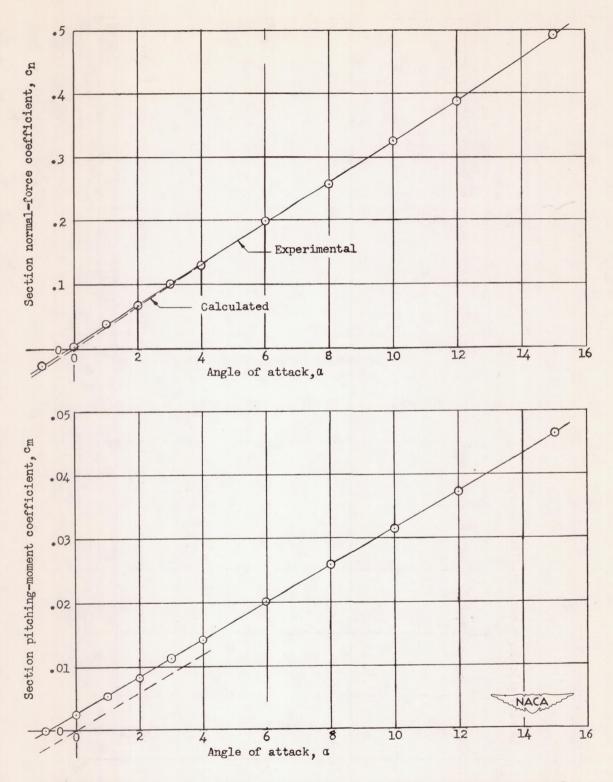
Figure 8.- Effect of angle of attack on section normal-force and
pitching-moment coefficients for NACA 65-009. M = 2.40;
R = 0.81 × 10⁶.
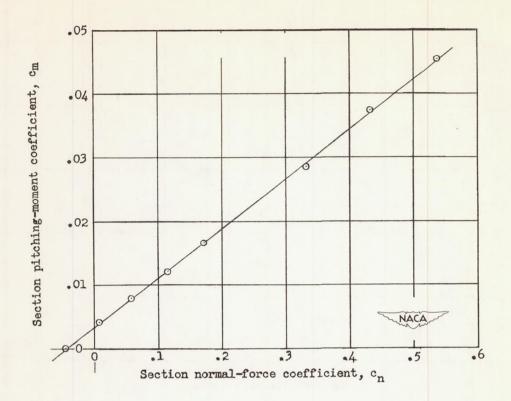
Figure 9.- Variation of c_m with c_n. M = 1.62; R = 1.07 × 10⁶.
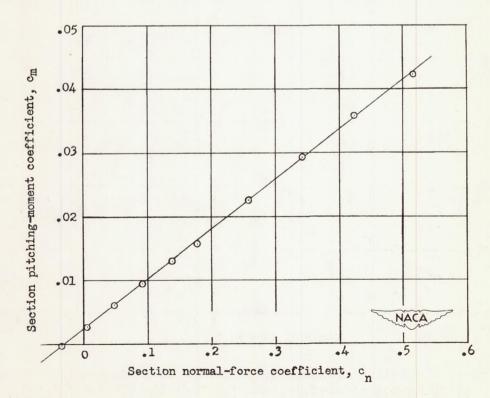
Figure 10.- Variation of c_m with c_n. M = 1.93; R = 0.97 × 10⁶.
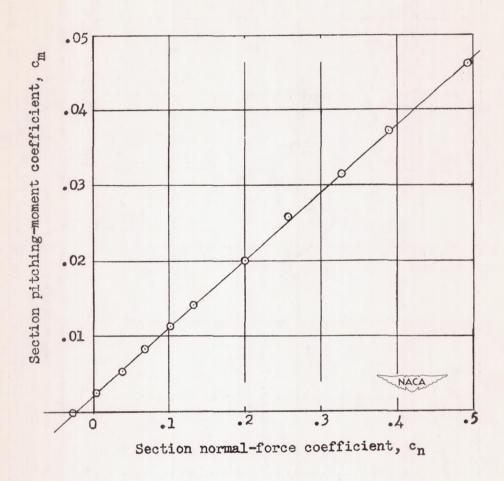
Figure 11.- Variation of c_m with c_n. M = 2.40; R = 0.81 × 10^6.
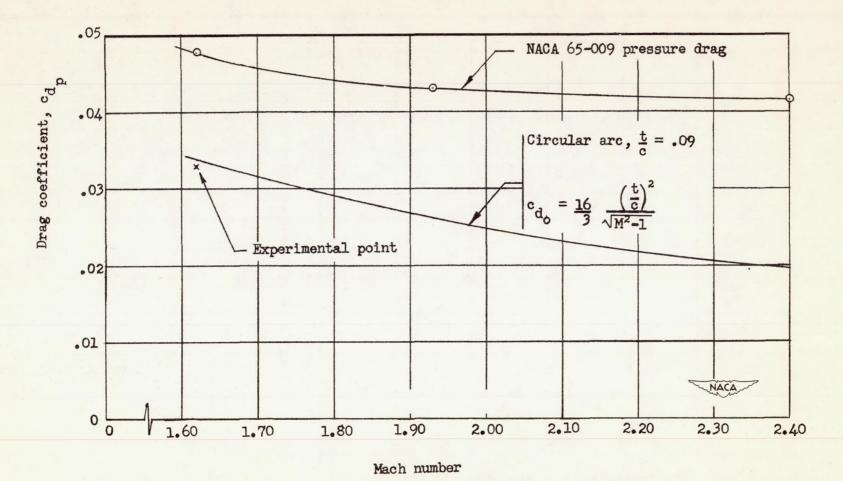
Figure 12.- Pressure drag coefficients at various Mach numbers of NACA 65-009 and symmetrical circular-arc airfoils.
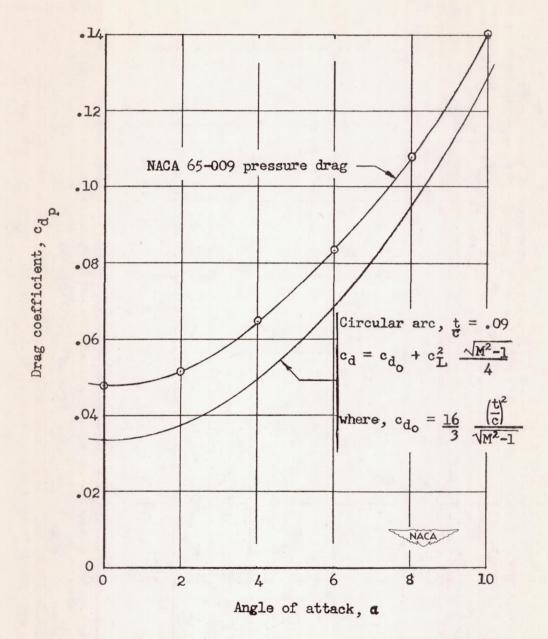
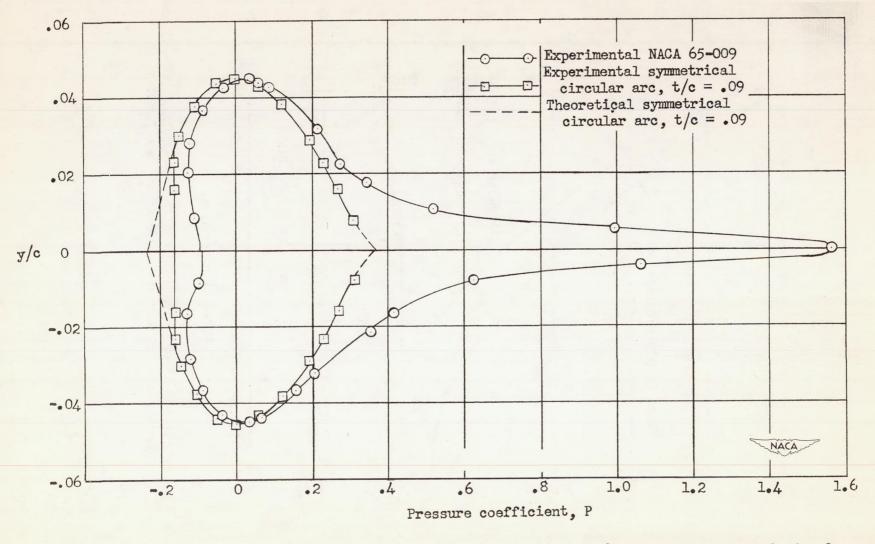Figure 13.- Comparison of pressure drag coefficients of NACA 65-009 and symmetrical circular-arc airfoils at M = 1.62.
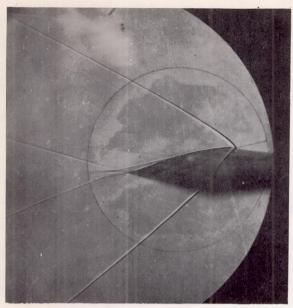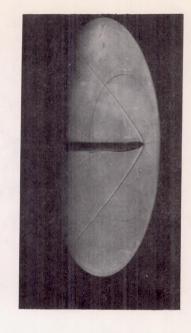
Figure 14.- Comparison of chordwise pressure distributions of NACA 65-009 and symmetrical circular-arc airfoils at $\alpha = 0°$ and $M = 1.62$.

(a) Rear three-quarter view.   (b) Front three-quarter view.

Figure 15.- Shadowgraphs of flow past NACA 65-009 airfoil. $\alpha = 10^{\circ}$;
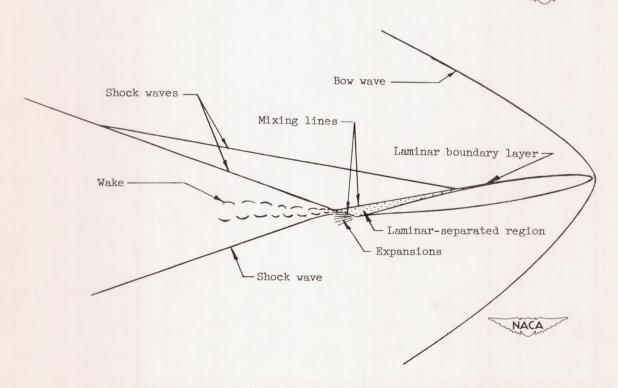$M = 2.40$; $R = 0.81 \times 10^{6}$.

Figure 16.- Schematic drawing of shadowgraphs indicating character
of flow about NACA 65-009 airfoil. $\alpha = 10^{\circ}$; $M = 2.40$;
$R = 0.81 \times 10^{6}$.